NUMERICAL ANALYSIS OF UNBONDED POST-TENSIONED REINFORCED CONCRETE BEAMS FOR RESILIENCY EVALUATION

O. Inui [(1)], T. Obara [(2)], S. Kono [(3)], D. Mukai [(4)]

[(1)] *Graduate student, Tokyo Institute of Technology, Japan, inui.o.aa@m.titech.ac.jp*
[(2)] *Assistant professor, Institute of Innovative Research, Tokyo Institute of Technology, Japan, obara.t.ac@m.titech.ac.jp*
[(3)] *Professor, Institute of Innovative Research, Tokyo Institute of Technology, Japan, kono.s.ae@m.titech.ac.jp*
[(4)] *Associate professor, University of Wyoming, USA, dmukai@uwyo.edu*

Abstract

Many reinforced concrete buildings designed based on recent seismic codes survived severe earthquakes such as the 2011 Tohoku earthquake and the 2016 Kumamoto earthquake from a collapse prevention view point. However, some buildings needed to be demolished due to damage to structural and non-structural members. The society in urban areas expects quick recovery or continuous use of buildings with their original functions intact after earthquakes. Thus it is important to develop low-damage structural system concepts and establish their design procedures. A self-centering rocking system using unbonded post-tensioning technology makes it possible to keep the original functions of buildings during and after hazards. Similarly, post-tensioned reinforced concrete (PRC) beams are frequently used to decrease displacement response and increase load carrying capacity of members. Experiments were conducted in 2014 on three PRC beams with and without slabs and with varying amounts of reinforcement. All specimens showed flag-shaped hysteretic loops with good self-centering characteristics and large energy dissipation. Due to the presence of longitudinal mild reinforcement, which increased the moment capacity, the PRC beams had flexural cracks.

This paper describes numerical analyses to evaluate damage of three PRC beam specimens with or without slabs (PRC1, 2, 3) using a relatively simple multi-spring model. The model consists of multi spring elements for flexural behavior and elastic spring elements for shear behavior. Each material is assigned each constitutive relationship which has own stress-strain curve. The plastic length (Lp) are defined as half of beam height. The program SNAP is used for this elasto-plastic analysis.

The analytical model simulates shear force(Q) - drift angle ratio (R) relations, the behavior of PC tendons tension force, and equivalent damping ratio (heq) with good accuracy. The authors believe that is due to the envelope curves of each member being simulated precisely. This information will be helpful to evaluate structural function of PRC beams. However, the analytical model cannot capture the slab and longitudinal reinforcement strains and residual drift angle ratio. These are for future consideration.

Keywords: Unbonded post-tensioned reinforced concrete beam, Multi-spring model, Residual drift angle ratio, Equivalent damping ratio

1. Introduction

Even if a building didn't collapse during disastrous earthquakes in Japan in the past, it was impossible to continue to occupy many buildings due to damage of structural and non-structural members. This economic loss from downtime may be larger than repair costs for damage the building suffered during the earthquake. Therefore, societal demands in recent years have shifted to a structural system that suppresses damage during an earthquake as much as possible and enables quick recovery and continuous use of the building after an earthquake. Against these demands, pre-stressed reinforced concrete (PRC) structures can maintain flexural strength sufficiently and form the basis of damage-control structural systems that minimize damage of members. That is, it is possible to construct a structural system which has an ideal flag-shaped hysteretic behavior with large energy dissipation and a small residual deformation after an earthquake.

In this paper, we focus on unbonded post-tensioned reinforced concrete beams which can realize flag-shaped hysteretic behavior and conduct an analytical performance evaluation. Moriguchi et al. [2] focused on the damage evaluation of slab reinforcement in six unbonded PRC beams with slabs that he previously tested. Kishimoto et al. [3] conducted a parametric study with variable steel ratios and using fiber-based model analysis to evaluate hysteretic behavior and equivalent damping ratio quantitatively. Watanabe et al. [4] proposed a sectional analysis model for unbonded precast pre-stressed concrete and simulated the damage of experimental results.

On the other hand, there are less papers that quantitatively evaluate parameters such as width of cracks and limit states of PRC beams. Therefore, the objective of this paper is to construct an analysis model of unbonded PRC beams which have high resiliency function and quick recovery. A primary goal of the research is to develop an analysis method which can estimate the damage state quantitatively. To this end, the experimental results of three unbonded PRC beams whose static testing was conducted by Moriguchi et al.[3] are modeled using a relatively simple multi-spring model. The model results are compared to the experimental results to determine the accuracy of the model and the effectiveness of the model at capturing material-level response.

2. Modeling using multi-spring model

We propose an analysis method using a multi-spring model to model three unbonded PRC beams in paper [2] (in Japanese).

2.1 Target specimen details

The parameters and details of the three unbonded PRC beams are given in Table 1, the mechanical characteristics of concrete and steel are presented in Table 2, and the arrangement and size of the specimens are shown in Figure 1. All three beams have a 500mm width and 600mm height, and the distance between the fixed end of the beam and the loading point is 1800mm. Only PRC1 (slab reinforcement reaches to stub) and PRC2 (slab reinforcement doesn't reach to stub) have slabs which have a 100mm thickness and 1500mm width, with 800mm long slab reinforcement in the stub. PRC3 has the same properties as PRC1 and PRC2 except it does not have a slab. All beams had the same arrangement of reinforcements and were designed to fail in flexure. Stub, beam, and slab were casted monolithically.

Figure 2 shows the loading devices. The stub was fixed to the floor through an elevated pedestal (455mm height) and tensioned by a PC tendon. The drift angle ratio R, which is the vertical displacement at the loading point divided by the distance between fixed end of the beam and the loading point, was controlled during loading (displacement controlled).

2.2 Modeling unbonded PRC beams

Figure 3 shows the elevation of the analysis model. The model was divided into stub, plastic hinge zone and elastic beam area. Plastic hinge zone is defined as the area Lp from the fixed end of the beam and models the non-linear characteristics of material. We defined Lp as half of beam height (Lp=300mm) based on the paper by Watanabe and used a multi-spring model which can evaluate the interaction of axial load and bending moment in this Lp zone.

Table 1 – Parameter and details of unbonded PRC beams

Names			PRC1	PRC2	PRC3
Type			PRC		
Cross Section			With Slab		Without Slab
Characteristic Strength of Concrete			$60N/mm^2$		
Beam	Width×height		500mm×600mm		
	Longitudinal Reinforcement		4-D19(SD345)		
	PC Tendon		4-Φ26(C-1)		
	Sheath Tube		#1050		
	Stirrup	Main	D10(SD295A)@100(pw=0.51%)		
		Cross			
Slab	Thickness		100mm		
	Width		500mm×600mm		
	Slab Reinforcement		12-D6(SD295A)@150		
	Reaches to Stub		With	Without	
Shear Span Ratio (M/Qd)			3.0		
Steel Coefficient (q)			0.17		
Pre-stressed Ratio (λ)			0.62	0.68	0.68
Initial Tension Force			2000kN	1944kN	2020kN

Table 2 – Characteristic of each material

(a) Concrete

Specimens	f_c (N/mm^2)	ε_c (%)	E_c (kN/mm^2)
PRC1	69.6	4.36	34.3
PRC2	72.7	4.79	34.8
PRC3	69.0	5.23	34.6

f_c:Compression Stress, ε_c:Corresponding Strain, E_c:Young's Modulus

(b) Steel

	Diameter (Standard)	f_y (N/mm^2)	ε_y: (%)	f_s (N/mm^2)	E_s: (kN/mm^2)
Rebar	D19(SD345)	386	0.208	579	186
	D10(SD295A)	387	0.205	545	189
	D6(SD295A)	397	0.203	533	195
PC Tendon	φ26(C-1)	1179	0.770	1265	205

f_y:Yielding Stress, ε_y:Yielding Strain, f_s:Ultimate Stress, E_s:Young's Modulus

The vertical displacement of the free end of the beam and the fixed end bending moment were calculated using non-linear analysis. As shown in Figure 3, elasto-plastic spring elements, elastic beam elements and rigid beam elements were used to model the Lp zone, the portion of the beam beyond Lp, and the stub, respectively. Figure 4 shows the cross-section of the multi-spring model used for PRC1. PRC2 was modeled without slab reinforcement and PRC3 was modeled without the slab.

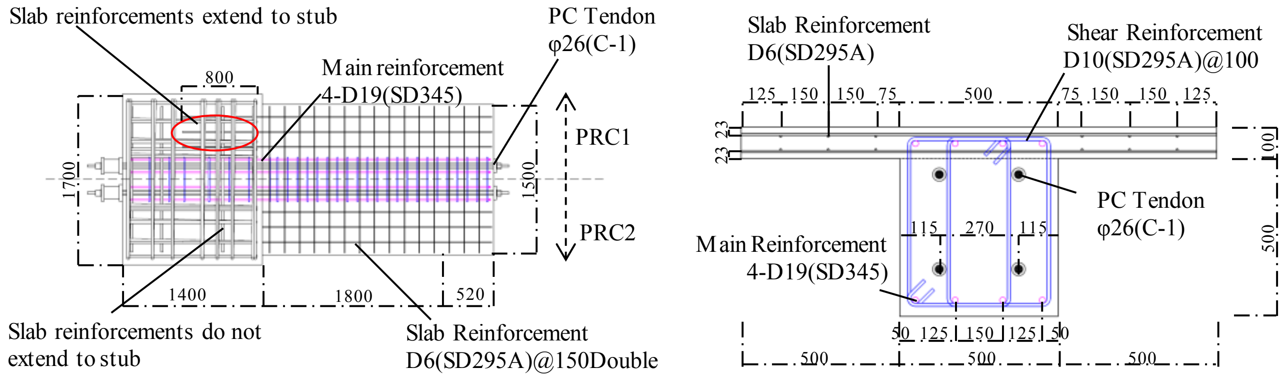

(a) Plan [PRC1 and PRC2]

(a) Section [PRC1 and PRC2]

Fig. 1 – Arrengement of rebars and Size of specimens

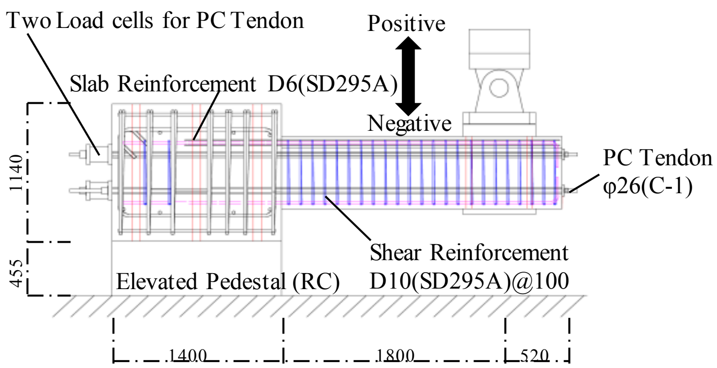

Fig. 2 – Loading Setup

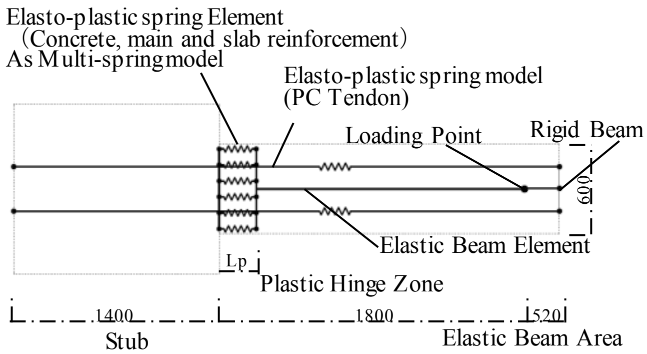

Fig. 3 – Elevation of analysis model

In the plastic hinge zone, elasto-plastic spring elements replaced the concrete and reinforcement elements. For PC tendon, an elasto-plastic spring element which has the length along the entire specimen was placed in parallel to the beam and stub elements. Longitudinal reinforcements were modeled with an assumption of non-slip condition. The initial forces in the PC tendons were taken as the values in the experiment. After applying initial pre-stress, loading was applied by controlling the displacement of the free end of the cantilever beam. In this analysis, we focused on the damage evaluation up until a drift angle ratio of ±4.0% where no fractures were observed in the experiment. The program SNAP was used for this elasto-plastic analysis.

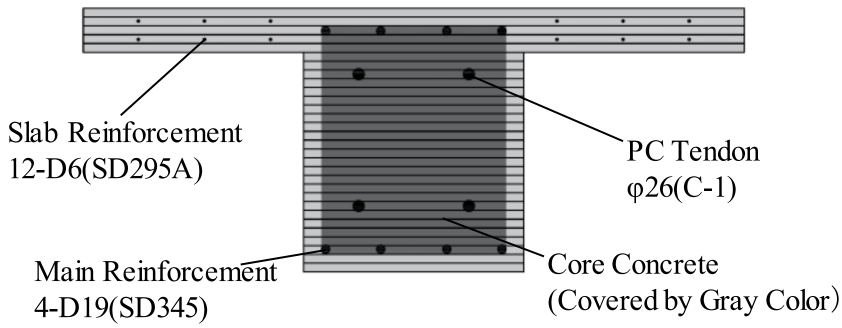

Fig. 4 – Cross-section of multi-spring model

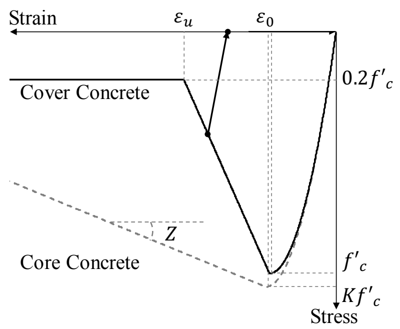

(a) Compression of Concrete

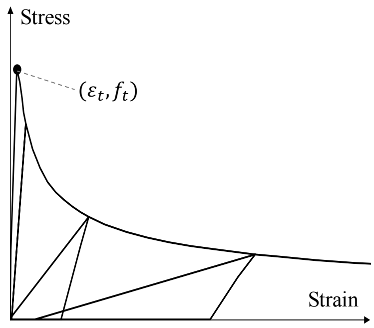

(b) Tension of Concrete

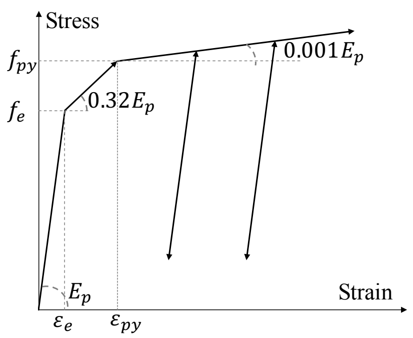

(C) PC tendon

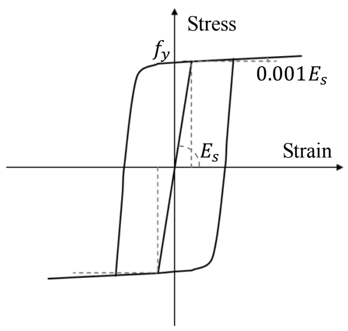

(d) longitudinal and slab reinforcement

Fig. 5 – Stress–Strain Curves of each materials

2.3 Constitutive Relationship

Figure 5 shows the stress-strain curves for concrete, PC tendon, and reinforcement used in this analysis (positive is tension, negative is compression). The concrete was divided into cover concrete and core concrete which was confined by the transverse shear hoops. The cover concrete used a modified Kent-Park model with an ultimate strain as 0.007. The core concrete also used a modified Kent-Park model and the same ultimate strain and considered the confining effect of the hoops. On the tension side, cracking stress was calculated using Eq. (1)[6], and strain at the peak stress was defined as ε_t=0.05%. A tri-linear envelope curve was used to model the PC tendon. The stiffness reduction ratio after yielding was taken as 0.001. A bi-linear envelope curve and modified Ramberg-Osgood model for hysteresis characteristics were used to model the longitudinal reinforcement and slab reinforcement. The values from material test results were used for the material properties of each model.

$$f_t = 0.33\sqrt{f_c'} \quad \text{[MPa]} \tag{1}$$

where f_c' is compression stress of concrete [MPa]

3. Analysis results and Comparison to experiment

3.1 Shear force(Q)-Drift angle ratio(R) relation

Figure 6 shows shear force (Q)-drift angle ratio(R) relations obtained by analysis and experiment along with each peak force. Table 3 shows the comparison between the experimental values and the analytical values at the maximum force point. In the positive direction, the maximum shear force and drift angle ratio from analysis were close to the experimental values and were conservative. In the negative direction, the analysis maximum shear force was close to the experimental results, but slightly unconservative. Both the envelop curve and unloading stiffness were simulated with good accuracy until R=4.0% in the positive direction.

However, the unloading hysteresis behavior past R=1.0% in the negative direction did not simulate the experimental result precisely. Especially in the negative direction, the residual deformation from the analysis did not match the experimental result. The analysis hysteresis behavior of all three specimens showed smaller residual deformation than the experiment.

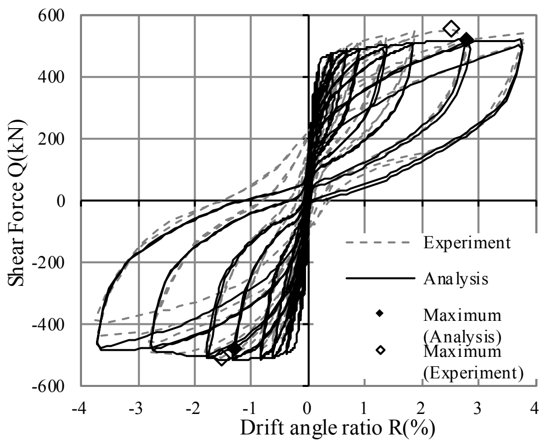

(a) PRC1

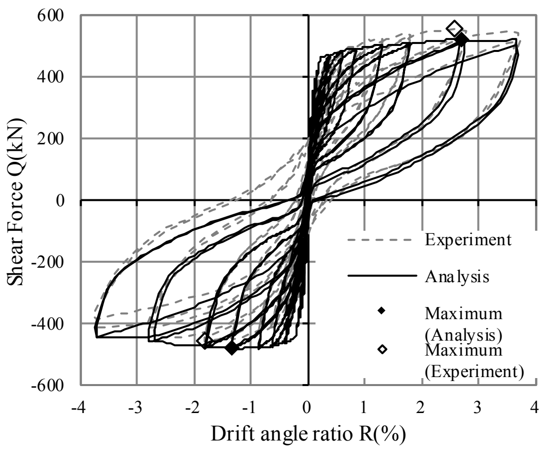

(b) PRC2

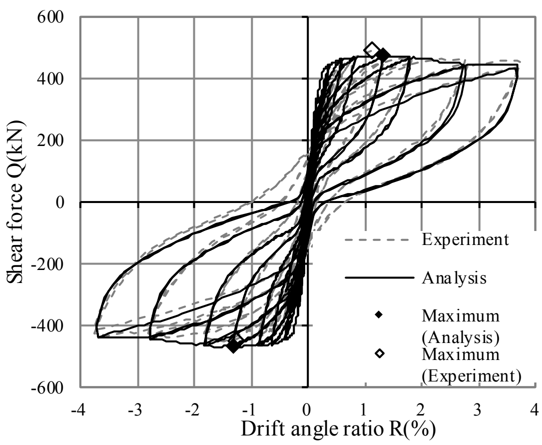

(c) PRC3

Fig. 6 – Shear force(Q) - Drift angle ratio(R) relations

Table 3 – Comparison of maximum force

		Positive		Negative	
		Q[kN]	R[%]	Q[kN]	R[%]
PRC1	Experiment	554	2.50	-509	-1.54
	Analysis	522	2.76	-518	-1.32
	Experiment/Analysis	1.06	0.91	0.98	1.17
PRC2	Experiment	554	2.57	-461	-1.83
	Analysis	523	2.68	-485	-1.35
	Experiment/Analysis	1.06	0.96	0.95	1.36
PRC3	Experiment	490	1.12	-456	-1.26
	Analysis	477	1.32	-472	-1.33
	Experiment/Analysis	1.03	0.85	0.97	0.95

3.2 Behavior of PC tendon

Figure 7 shows the PC tendon tension force-drift angle ratio(R) relations of PR1 and PRC3. PRC2 is omitted due to a similar response to PRC1. The value obtained from the load cell at the end of stub in the experiment was used to determine the PC tendon force. Green and red dashed lines in Figure 7 show the elastic limit (0.02% offset strength) and yield stress (Table 2), respectively. Up to R=3.0% in all specimens, the experimental results including the hysteresis loops in unloading could be simulated with good accuracy. Additionally, since the envelop curves almost matched the experiment results, the envelop curves in Figure 6 were also accurately simulated. However, the behavior of PC tension force could not be simulated after R=3.0% and the analysis showed the lower values than the experiment results.

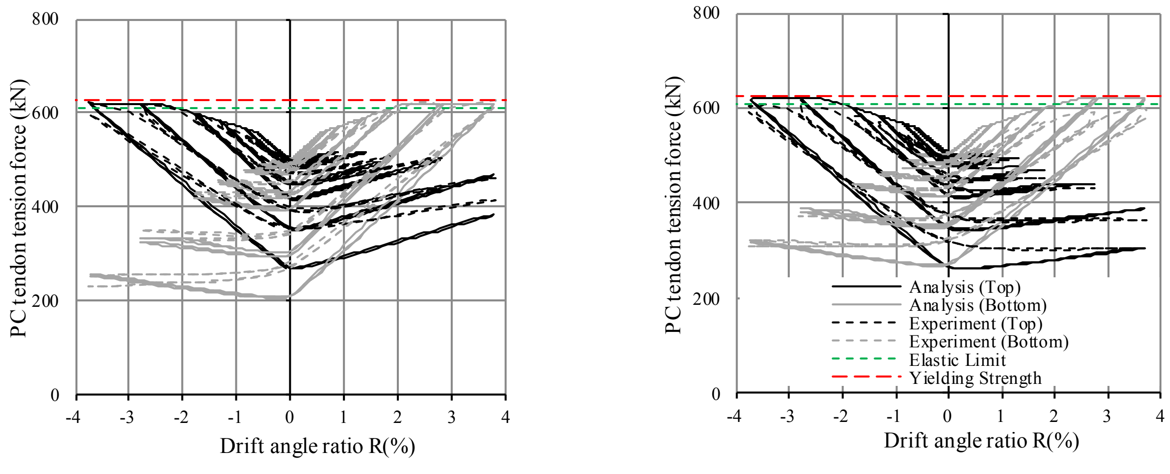

(a) PRC1 (b) PRC3

Fig. 7 – PC tension force - Drift angle ratio(R) relations

3.3 Behavior of slab and longitudinal reinforcement

Figure 8a shows the slab reinforcement strain – drift angle ratio (R) relation, and Figure 8b shows the longitudinal reinforcement strain – drift angle ratio (R) relation in PRC1. The strain values in the experiment were obtained by strain gauges put at critical sections. In Figure 8a and 8b, the strains in the experiment were well behaved until yielding at R=-0.75% to R=-1.0%. After that, strains when loading in the negative direction increased dramatically with large strain hysteresis loops. In contrast, in the analysis even if the slab and longitudinal reinforcement yielded, the loading path was identical for all cycles in loading and unloading and the hysteresis behavior in the experimental results could not be simulated. In the experiment, cracks occurred in the fixed end of the beam and if some degree of bond remained, the strain became larger locally at the critical section as shown in Figures 8a and 8b. In the multi-spring model, this concentration local strain and stress occurring in the experiment could not be simulated because the strains were averaged over the plastic hinge zone.

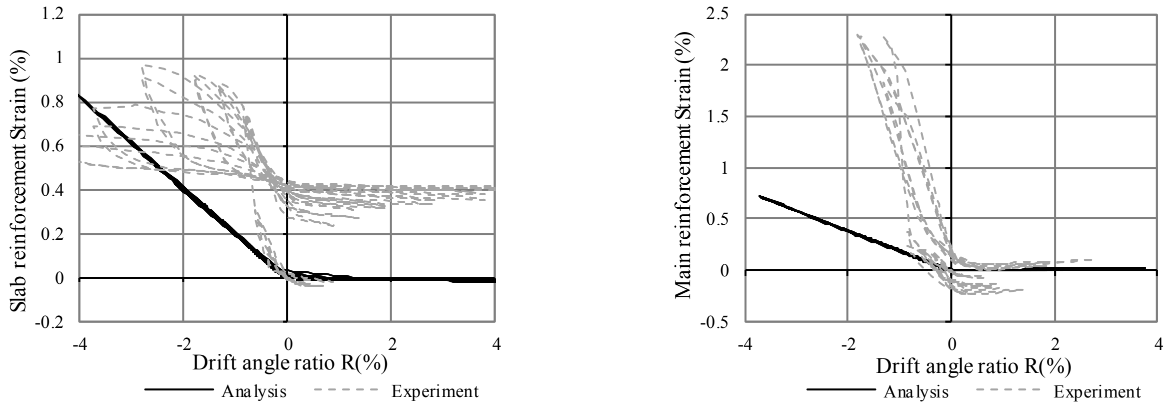

(a) Slab reinforcement (b) Longitudinal reinforcement

Fig. 8 – Reinforcement Strain – Drift angle ratio (R) relations [PRC1]

3.4 Residual drift angle ratio

Figure 9 shows residual drift angle ratio – drift angle ratio (R) relations in PRC1 and PRC2. PRC3 is omitted due to similar response to PRC2. The drift angle ratio when the horizontal force acting on the beam equaled 0 was used as the residual angle ratio. This was calculated using the second hysteresis response of each cycle in both the analysis and experiment.

In both specimens, the residual angle ratios were less than 0.4% until R=2.0% in both the analysis and experiment. In PRC1, the experimental results could be captured until R=4.0% accurately. In PRC2, although close agreement with the experimental results could be simulated from R=0.25% to R=1.0%, the slope of the analysis was higher than the experimental results after R=-1.0%. The behavior of PRC2 in the experiment could not be simulated because the analytical response returned to 0 after R=3.0% as shown in Figure 6.

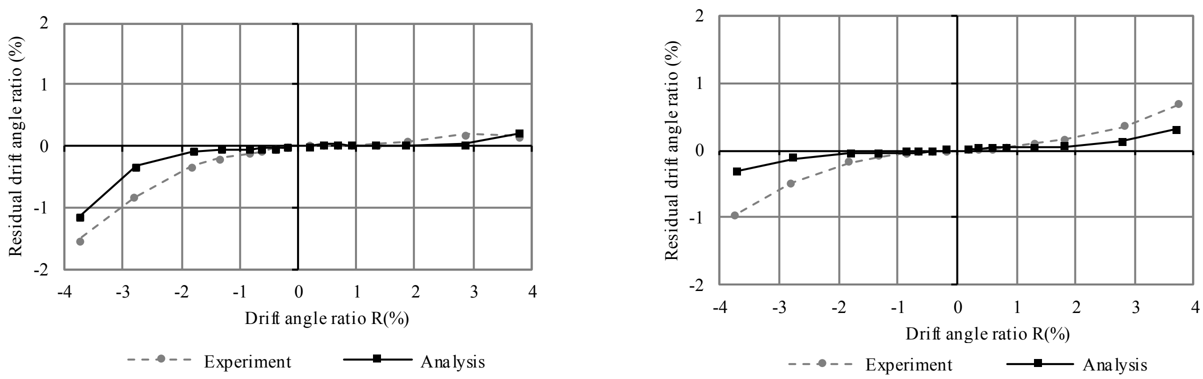

(a) PRC1 (b) PRC2

Fig. 9 – Residual drift angle ratio – Drift angle ratio (R) relations

3.5 Equivalent damping ratio h_{eq}

Figure 10 shows the equivalent damping ratio (h_{eq}) – drift angle ratio (R) relations for PRC1 and PRC2. PRC3 is omitted due to similar behavior to PRC2. Equivalent damping ratio is calculated based on reference [7]. In this section, Eq.(2) is used for a half cycle because the resisting mechanism are different for positive and negative. This is calculated using the second hysteresis response of each cycle in both the analysis and experiment.

$$h_{eq} = \frac{1}{2\pi}\left(\frac{\Delta W}{W_e}\right) \tag{2}$$

where ΔW is area of hysteresis loop in a cycle, W_e is equivalent potential energy

In both specimens, the analytical results could be simulated accurately until R=4.0%. The value of h_{eq} was 13~15% until R=2.0%, which matches the experimental results. In PRC1, the analytical result was higher than the experimental result, making the model unconservative.

The experimental results are simulated accurately (Fig. 10) as the numerical model could reproduce the experimental envelope curve of each member. In addition, PRC1 which had slab reinforcement developed and anchored in the stub, tended to have bigger h_{eq} than PRC2 in which the slab reinforcement was curtailed in the slab and not anchored in the stub. The experimental results also showed similar behavior, thus we could reproduce the effect of slab reinforcement in the analysis.

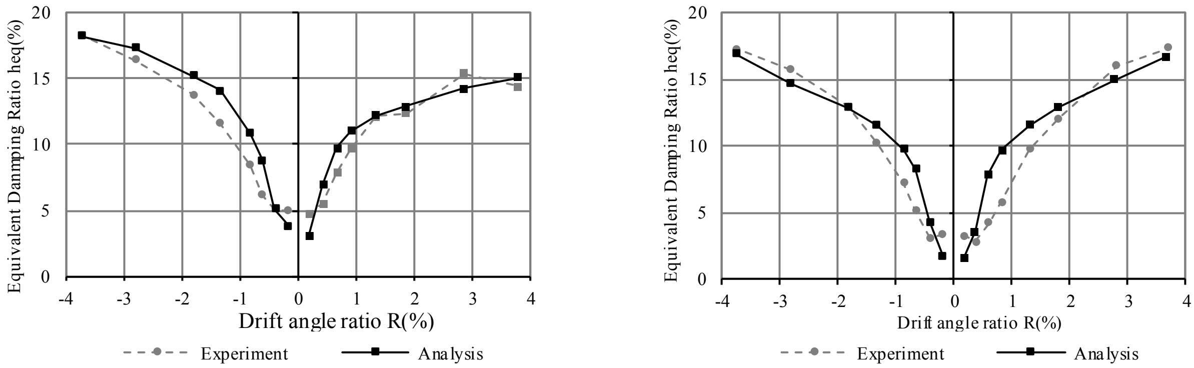

(a) PRC1 (b) PRC2

Fig. 10 – Equivalent damping ratio (h_{eq}) – Drift angle ratio (R) relations

4. Conclusions

In this paper, we proposed an analysis method using a multi-spring model and tried to simulate the experimental results for three unbonded PRC beams subjected to static loading experiments. By assuming that the plastic hinge zone Lp is half of the beam height, shear force (Q) – drift angle ratio (R) relations, the behavior of PC tendon stress and equivalent damping ratio could be simulated with good accuracy.

However, the experimental results of the slab and longitudinal reinforcement strains and residual drift angle ratio could not be captured by this model. These are for future consideration.

5. Acknowledgements

This work was supported financially by JSPS through their Grant-in-Aid program (PI: S. Kono). We are also thankful to the Collaborative Research Project (Materials and Structures Laboratory), and the World Research Hub Initiative (Institute of Innovative Research), at Tokyo Institute of Technology for their generous support of this work.

6. Copyrights

7. References

[1] NILIM and BRI (2012): Report of damage investigation due to the 2011 off the Pacific coast of Tohoku Earthquake. Vol.674 (NILIM) and Vol.136 (BRI) [In Japanese]

[2] Kishimoto I, Oono Y (2002): Analytical investigation of energy absorption capacity of prestressed concrete beam, Proceedings of the Japan Concrete Institute, Vol.24-2, pp.643-648 [In Japanese]

[3] Moriguchi Y, Miyamoto K, Kono S, Watanabe H, Takenaka H, Takamori N, Hirata N, Fujii A, Kim D, Egashira H, Hiwatashi T, Okayasu T (2014): Experimental study on flexural behavior of unbonded prestressed concrete beams with slab, Summaries of Technical Papers of Annual Meeting, Architectural Institute of Japan, pp.749-752 [In Japanese]

[4] Watanabe H, Moriguchi Y, Obara T, Kono S, Takenaka H (2016): Damage evaluation of precast concrete beams post-tensioned with unbonded tendons using fiber based model analysis, Journal of Structural and Construction Engineering (Transactions of AIJ), No.729, pp.1921-1931 [In Japanese]

[5] Structure System Corp. (2019): Elastic and plastic analytic program of Three-dimensional frame, SNAP Ver.7 [In Japanese]

[6] Architectural Institute of Japan (2004): Guidelines for performance evaluation of earthquake resistant reinforced concrete buildings [In Japanese]

[7] Shibata A (2014): Dynamic Analysis of Earthquake Resistant Structures, Morikita Publishing [In Japanese]